Clinically approved IVIg delivered to the hippocampus with focused ultrasound promotes neurogenesis in a model of Alzheimer's disease

Sonam Dubey[a,b], Stefan Heinen[a] , Slavica Krantic[c], JoAnne McLaurin[a,b], Donald R. Branch[d] , Kullervo Hynynen[e,f], and Isabelle Aubert[a,b,1]

[a]Biological Sciences, Hurvitz Brain Sciences Research Program, Sunnybrook Research Institute, Sunnybrook Health Sciences Centre, Toronto, ON M4N 3M5, Canada; [b]Laboratory Medicine and Pathobiology, Temerty Faculty of Medicine, University of Toronto, Toronto, ON M5S 1A1, Canada; [c]Sorbonne Université, Inserm, Centre de Recherche Saint-Antoine, CRSA, F-75012 Paris, France; [d]Centre for Innovation, Canadian Blood Services, Toronto, ON M5G 2M1, Canada; [e]Physical Sciences, Sunnybrook Research Institute, Sunnybrook Health Sciences Centre, Toronto, ON M4N 3M5, Canada; and [f]Medical Biophysics, Temerty Faculty of Medicine, University of Toronto, Toronto, ON M5S 1A1, Canada

Preclinical and clinical data support the use of focused ultrasound (FUS), in the presence of intravenously injected microbubbles, to safely and transiently increase the permeability of the blood–brain barrier (BBB). FUS-induced BBB permeability has been shown to enhance the bioavailability of administered intravenous therapeutics to the brain. Ideal therapeutics candidates for this mode of delivery are those capable of inducing benefits peripherally following intravenous injection and in the brain at FUS-targeted areas. In Alzheimer's disease, intravenous immunoglobulin (IVIg), a fractionated human blood product containing polyclonal antibodies, act as immunomodulator peripherally and centrally, and it can reduce amyloid pathology in the brain. Using the TgCRND8 mouse model of amyloidosis, we tested whether FUS can improve the delivery of IVIg, administered intravenously (0.4 g/kg), to the hippocampus and reach an effective dose to reduce amyloid plaque pathology and promote neurogenesis. Our results show that FUS-induced BBB permeability is required to deliver a significant amount of IVIg (489 ng/mg) to the targeted hippocampus of TgCRN8 mice. Two IVIg-FUS treatments, administered at days 1 and 8, significantly increased hippocampal neurogenesis by 4-, 3-, and 1.5-fold in comparison to saline, IVIg alone, and FUS alone, respectively. Amyloid plaque pathology was significantly reduced in all treatment groups: IVIg alone, FUS alone, and IVIg-FUS. Putative factors promoting neurogenesis in response to IVIg-FUS include the down-regulation of the proinflammatory cytokine TNF-α in the hippocampus. In summary, FUS was required to deliver an effective dose of IVIg to promote hippocampal neurogenesis and modulate the inflammatory milieu.

MRI-guided focused ultrasound | blood–brain barrier | immunotherapy | intravenous immunoglobulin | neurogenesis

Alzheimer's disease (AD) is a neurodegenerative disease estimated to affect 132 million individuals worldwide by 2050. The incidence of AD significantly increases with age, with 1 in 10 people over 65-y old being affected (1). At present, AD has no cure and the multifaceted nature of this disorder prompts the development of therapeutics that can both reduce pathologies and promote the regenerative capacity of the brain (2, 3).

One such therapeutic is intravenous immunoglobulin (IVIg). IVIg is composed of pooled antibodies collected from healthy blood donors that have been shown, in patients with AD and animal models of AD, to decrease amyloid-β peptides (Aβ) and tau pathology, dampen excessive inflammation, and increase neurogenesis (4–12). The excellent safety profile of IVIg combined with its beneficial effects, in animal models and early clinical AD trials, led to a phase III trial in patients with mild to moderate AD (13, 14). The phase III clinical trial failed to demonstrate significant cognitive improvement in the overall population treated, although a subgroup analysis pointed to

some benefits in apolipoprotein-E4 carriers and at moderate AD stages (9, 13–15).

The properties of the blood–brain barrier (BBB) restrict the bioavailability of IVIg to the brain. While technically difficult to evaluate in human, studies in murine models of AD have shown that less than 0.002% of IVIg reach the hippocampus (9, 16). Using higher dosages to increase the amount of IVIg to the brain has limitations, both in terms of safety and feasibility. Clinically, IVIg is used for several autoimmune and inflammatory conditions, and its expansion to AD at relatively high dosages could put a serious burden on the provision of IVIg, a human source biologic (17, 18). As such, strategies are warranted to develop recombinant alternatives to IVIg (19), reduce the amount of IVIg required, and combine IVIg with new therapeutic and delivery approaches to increase efficacy. The present study contributes to efforts in improving treatment efficacy by enhancing the delivery of IVIg to the brain using focused ultrasound (FUS), keeping a relatively low dose of IVIg, and potentially benefiting from FUS-induced effects in reducing pathology and increasing neurogenesis (20–23).

Since 2001, MRI-guided FUS combined with intravenously administered microbubbles has been established as a modality to

Significance

The efficacy of immunotherapy in Alzheimer's disease is limited, partly because antibodies, administered peripherally, have poor access to the brain. Focused ultrasound (FUS) with microbubbles allows the passage of antibodies from the blood to the brain. In a mouse model of Alzheimer's disease, antibodies administered in the blood, with and without FUS, reduced amyloid pathology. In contrast, FUS was required to deliver sufficient antibodies to the hippocampus and effectively promote neurogenesis. Neurogenesis, a regenerative process involved in memory functions, is impaired in Alzheimer's disease. Putative contributors to the stimulation of neurogenesis include a decrease in the proinflammatory cytokine TNF-α. FUS holds potential to increase the efficacy of immunotherapy for Alzheimer's disease.

increase the permeability of the BBB (24). The use of well-defined FUS parameters, microbubble dosage, an acoustic emissions-based controller, and MRI guidance provides assurance in real-time that FUS-induced BBB permeability is done in a safe, reproducible, and targeted manner (24–30). FUS-mediated drug delivery requires the administration of therapeutics intravenously to facilitate their passage through the BBB and into the brain at FUS-targeted regions. Therefore, therapeutics that are beneficial centrally and peripherally, such as IVIg (9, 18), are ideal candidates to combine with FUS-mediated drug delivery. To date, molecules, cells, and gene vectors have been shown to be effectively delivered using FUS (27). In animal models of AD, FUS-mediated drug delivery to the brain has been used for immmunotherapy against Aβ and tau pathologies (31–34), and for the delivery of a specific agonist stimulating TrkA signaling and acetylcholine release (3).

We hypothesized that FUS-induced BBB permeability would significantly enhance the delivery of IVIg from the blood to the hippocampus, a brain region vulnerable in AD (35), and thereby improve treatment efficacy. To test this hypothesis, we used the transgenic murine model of amyloidosis, namely TgCRND8, starting at 3 mo of age. At this age, TgCRND8 mice display salient features of AD, such as Aβ plaque burden (36), glial activation (37) associated with increased TNF-α (38), impaired hippocampal neurogenesis, and deficits in cogntive function (39, 40). As such, TgCRND8 mice at 3 mo of age model a clinical stage when patients would be presenting with pathological characteristics of AD, and prior to further neuronal systems degenerating (41, 42). Evidence suggests that treating AD at relatively early stages may be more efficient than at the later stages, when neurodegeneration reaches an irreversible stage (43).

In the present study, we first demonstrated the feasibility of IVIg delivery to the hippocampus using MRI-guided FUS in TgCRND8 mice. Next, we assessed the timeline of IVIg clearance from the brain. Finally, therapeutic efficacy of two weekly treatments of IVIg, FUS, and IVIg-FUS (at day 1 and day 8) was investigated 2 wk later, at day 21 on Aβ plaque pathology, neurogenesis, and the inflammatory status centrally, in the hippocampus, and peripherally, in the serum.

Results

FUS Increases the Bioavailability of IVIg to the Hippocampus. The bioavailability of IVIg delivered to the hippocampus with FUS was measured at 4 h, 24 h, 7 d, and 14 d posttreatment (Fig. 1A), in TgCRND8 (Tg) and nontransgenic (nTg) mice. Two FUS spots per region were chosen for targeting the left hippocampus, and as a supplementary region the frontal cortex (Fig. 1B). Under MRI-guidance, the left hippocampus and cortex were selected (Fig. 1C) and targeted with FUS (Fig. 1D). The contralateral right hemisphere served as non-FUS control side, allowing for paired comparison within animals. Both hippocampi were exposed to IVIg in the circulation (0.4 kg/kg, intravenously) and only the left hippocampus was targeted with FUS.

Immediately following FUS treatment in the presence of microbubbles (0.02 mL/kg), a gadolinium-based MRI contrast agent, Gadodiamide (GAD; 0.2 mL/kg) and IVIg (0.4 g/kg) were injected intravenously. To visualize the permeability of the BBB, post-FUS treatment T1-weighted (T1w) images (Fig. 1D) were compared to the pre-FUS T1w images (Fig. 1C). BBB permeability at the target locations was confirmed by GAD enhancement on T1w images post-FUS, as noted by the two lighter gray spots in the hippocampus and in the cortex in Fig. 1D compared to Fig. 1C. The levels of enhancement produced by GAD at FUS sites was not significantly different between Tg and nTg animals (Fig. 1E) ($n = 16$, $P = 0.21$), indicating that the levels of BBB permeability induced by FUS is comparable in Tg and nTg mice.

In Tg mice, IVIg at 0.4 g/kg (12 mg per mouse, intravenously) did not bypass the BBB in the absence of FUS (Fig. 1F, 4-h time-point) ($n = 6$, 0 ng/mg). In contrast, in FUS-targeted hippocampi the levels of IVIg detected 4 h posttreatment ranged from 67 to 1,013 ng/mg, and on average (489 ng/mg) significantly higher compared to the untreated side (average 0 ng/mg) (Fig. 1F) ($P = 0.016$, $n = 6$). Therefore, this bioavailability data demonstrate that one administration of IVIg-FUS delivered represents, on average, 0.09% (0.01 to 0.2%) of the injected dose to the targeted hippocampi. At 24 h post-FUS, IVIg remaining in the targeted hippocampi averaged 152 ng/mg (Fig. 1F) ($P = 0.063$ compared to the untreated side, average 0 ng/mg, $n = 6$). By 7
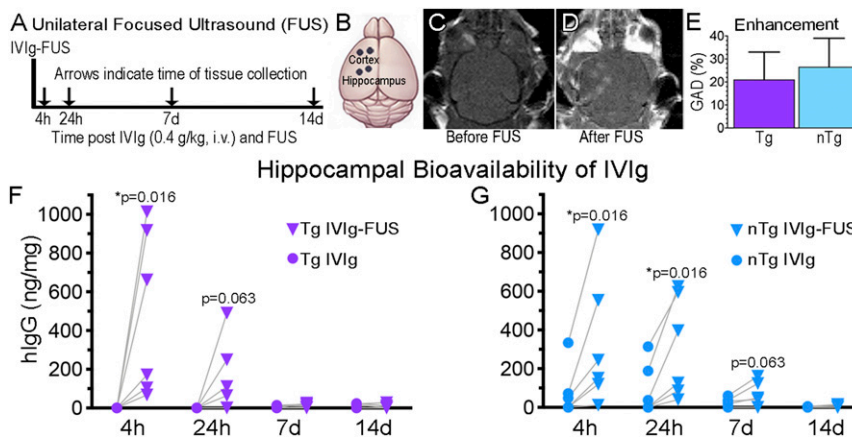

Fig. 1. FUS increases the bioavailability of IVIg to the hippocampus. (A–D) A unilateral FUS treatment. FUS was done on the left side of the brain. (A) IVIg (0.4 g/kg) was injected intravenously in Tg and nTg animals. Animals were killed at 4 h, 24 h, 7 d, and 14 d and brain homogenates were analyzed using human IgG (hIgG) ELISA. (B) The BBB was modulated with two FUS spots (black dots) per regions, namely the cortex and hippocampus. The contralateral regions on the right side of the brain served as controls exposed to circulating IVIg without FUS permeabilization. (C and D) MRI visualization of the brain (C) before and (D) after FUS-BBB opening, which results in noticeable GAD entry as two lighter spots over the cortex, and two over the hippocampus. (E) No significant difference in GAD enhancement post-FUS, indicative of BBB permeability, was observed between Tg and nTg animals ($n = 16$, $P = 0.21$). hIgG content was found to be higher in FUS-treated hippocampi (*Left*, triangles) compared to the untreated hippocampi (*Right*, circles) in Tg mice at 4 h after IVIg-FUS delivery (F, *$P = 0.016$, $n = 6$), and in nTg mice at 4 and 24 h treatment (G, *$P = 0.016$, $n = 6$ per time-point). GAD enhancement is represented as the mean+SD of all data points per group, with no statistical difference observed between groups. Bioavailability of IVIg at each independent time-point was analyzed with a Wilcoxon matched-pairs signed rank one-tail test, under the assumption that greater levels of IVIg will be found in FUS-treated hippocampi. Significant differences were noted at $P < 0.05$.

Dubey et al.

www.manaraa.com

and 14 d less than 20 ng/mg were detected on the FUS-treated hippocampus of Tg mice (Fig. 1*F*) (*n* = 6 per group).

In nTg animals, the levels of IVIg in the FUS-treated hippocampi averaged 333 ng/mg, ~0.06% of the injected dose, compared to 76 ng/mg on the contralateral untreated side (Fig. 1*G*) (*P* = 0.016, *n* = 6), and they remained elevated at 24 h in FUS-treated hippocampi (311 ng/mg) compared to the untreated side (90 ng/mg) (Fig. 1*G*) (*P* = 0.016, *n* = 6). The levels of IVIg remaining in the hippocampus post-FUS at 7 (62 ng/mg) and 14 (6 ng/mg) d were not statistically different from those observed on the contralateral side: Respectively, 24 ng/mg (Fig. 1*G*) (*P* =

0.063, *n* = 6) and 2 ng/mg (Fig. 1*G*) (*P* = 0.125, *n* = 6). The same trends were observed for the delivery of IVIg to the FUS-treated cortex of Tg and nTg mice (*SI Appendix*, Fig. S1) (*n* = 6 per group).

Treatment Efficacy. We next evaluated the biological effects of IVIg-FUS treatments on Aβ plaque pathology, neurogenesis, and inflammation. Bilateral hippocampal targeting was done for the following reasons: To cover the entire region for quantification of Aβ plaque pathology, to provide an appropriate sampling area for the estimation of the total number of cells
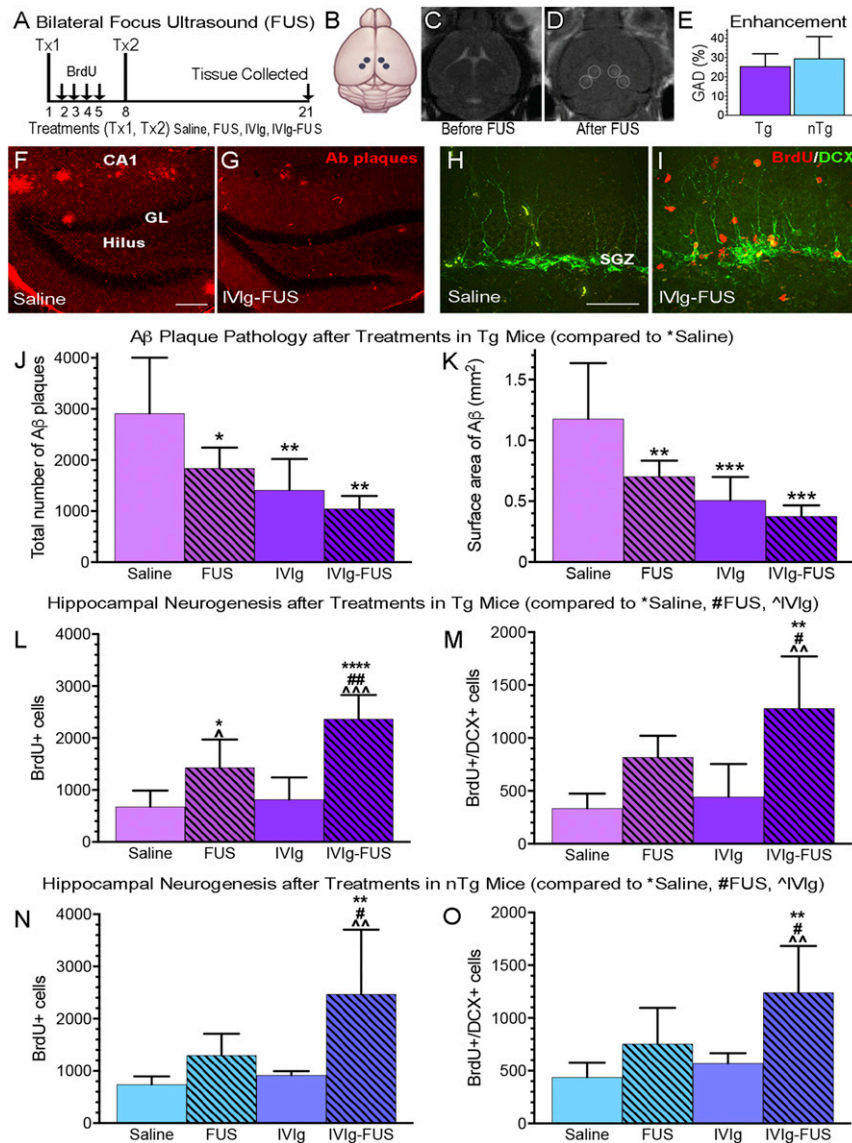

Fig. 2. IVIg reduces Aβ plaque pathology and promotes neurogenesis only when combined with FUS. (*A*) Experimental timeline of weekly bilateral treatments (Tx1, Tx2): Saline, IVIg alone (0.4 g/kg intravenously), FUS, IVIg-FUS at day 1 and 8, with tissue collection at day 21 in Tg and nTg animals. One day after the first treatment (Tx1), animals were injected intraperitoneally with BrdU (50 mg/kg) for 4 consecutive days (arrows) followed by a second treatment (Tx2) on day 8 and tissue collection on day 21. (*B*) The hippocampus was targeted bilaterally with four FUS spots. (*C* and *D*) MRI visualization of the brain (*C*) before and (*D*) after FUS-BBB opening, which results in noticeable GAD entry as four lighter spots over the bilateral hippocampi. (*E*) No significant difference in GAD enhancement post-FUS, indicative of BBB permeability, was observed between Tg and nTg animals (*P* = 0.33). (*F* and *G*) Representative images of plaques (red) in Tg mice treated with (*F*) saline and (*G*) IVIg-FUS. (Scale bar, 20 μm.) (*H* and *I*) Representative images of BrdU⁺ cells (red) and DCX⁺ cells (green) are shown here in nTg mice treated with (*H*) saline and (*I*) IVIg-FUS. (Scale bar, 100 μm.) (*J* and *K*) Aβ plaque number and surface area were significantly decreased by all treatments (FUS, IVI, and IVIg-FUS) compared to saline (*n* = 5 to 6 per group). No statistical difference was found in efficacy at reducing Aβ plaque pathology between treatments. (*L–O*) In Tg and nTg animals, IVIg-FUS was the most effective treatment at increasing (*L* and *M*) the total number of BrdU⁺ cells, and the only treatment to significantly increase (*N* and *O*) the number of immature neurons (BrdU⁺/DCX⁺) (*n* = 5). Data are shown as mean + SD with one-way ANOVA and Newman–Keuls post hoc tests. *,#,^*P* < 0.05, **,##,^^*P* < 0.01, ***,^^^*P* < 0.001, ****P* < 0.0001.

undergoing hippocampal neurogenesis per animal, and to globally treat the hippocampus for potential impact on serum cytokines, chemokines and trophic factors (CCTFs). Based on the clearance of IVIg at 7 d post-FUS treatment (Fig. 1 *F* and *G*), sex-balanced and age-matched Tg and nTg animals received two weekly treatments (Fig. 2 *A* and *B*), being allocated to one of four cohorts: Saline, IVIg, FUS, or IVIg-FUS. To confirm that the increased BBB permeability post-FUS is consistent between Tg and nTg animals, pre-T1w (Fig. 2*C*) and post-T1w (Fig. 2*D*) images were analyzed. The increase in GAD extravasation into the hippocampus, visualized as the hypointense regions in post-T1w images, was not significantly different between the FUS-treated Tg and nTg animals (Fig. 2*E*) (n = 10, P = 0.33). Therefore, differences in the biological effects observed under these conditions are unlikely to result from variability in the extent of FUS-mediated BBB permeability between Tg and nTg animals. Two weekly bilateral treatments of IVIg alone and IVIg-FUS resulted in the immunochemical detection of IVIg in the hippocampus, 14 d following the last treatment (*SI Appendix,*

Fig. S2 *A* and *B*). The detection of human-specific Ig-immunoreactivity in FUS-targeted hippocampi was higher compared to animals that received IVIg alone (intravenously without FUS) (P < 0.05) and saline (P < 0.01) (*SI Appendix,* Fig. S2 *A* and *B*). IVIg alone (intravenously without FUS) also led to detectable levels of human Ig, greater than those measured in the saline group (*SI Appendix,* Fig. S2 *A* and *B*) (P < 0.05). The immunopositive signal of IVIg in the hippocampus of Tg mice is diffuse (*SI Appendix, Fig. S2A*) with visible outlines of Aβ plaques (*SI Appendix, Fig. S2 A, d*, arrows), suggesting the binding of IVIg to plaques, and reminiscent of observations made by Puli et al. (10) in APP/PS1dE9 mice.

Aβ Plaque Pathology Is Reduced by All Treatments (IVIg, FUS, and IVIg-FUS). Aβ plaque pathology was quantified in the hippocampus of Tg animals (saline, Fig. 2*F*, and IVIg-FUS, Fig. 2*G*). A significant reduction in the number of hippocampal plaques was found following treatments with FUS (n = 5, P < 0.05), IVIg (n = 6, P < 0.01), and IVIg-FUS (n = 5, P < 0.01) compared to
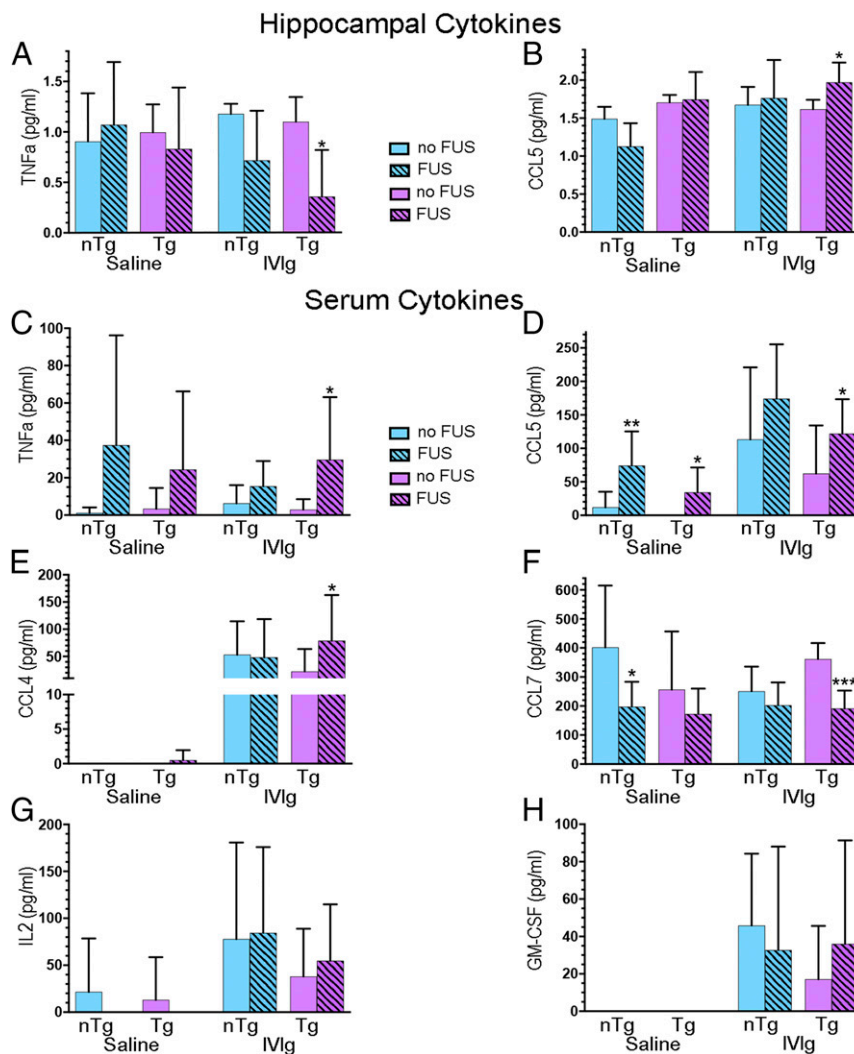

Fig. 3. IVIg-FUS treatments mediates changes in CCTF levels in the hippocampus and serum. (*A* and *B*) In Tg mice, IVIg-FUS treatments decreased TNF-α and increased CCL5 levels and in the hippocampus compared to IVIg treatment alone. (*C–E*) In the serum, Tg animals treated with IVIg-FUS show increased TNF-α, CCL5, and CCL4 compared to IVIg alone. CCL5 levels are also increased in FUS treated Tg and nTg animals (compared to saline). (*F*) Serum CCL7 is decreased with treatments of IVIg-FUS compared to IVIg in Tg animals, and with FUS treatments compared to saline in nTg animals. (*E, G,* and *H*) The detection of CCL4, IL-2, and GM-CSF was facilitated by IVIg and IVIg-FUS treatments in Tg and nTg animals. Hippocampal (n = 3 to 4) and serum (n = 9 to 15) CCTFs were analyzed using laser bead based multiplex assay for protein quantification. Data are shown as mean + SD with unpaired *t* test or Mann–Whitney *U* test. *P < 0.05, **P < 0.01, ***P < 0.001.

animals receiving saline (n = 5) (Fig. 2J). Similarly, the mean surface area (i.e., plaque load) was significantly lower in FUS (P < 0.01), IVIg (P < 0.001), and IVIg-FUS (P < 0.001) -treated animals compared to the saline group (Fig. 2K). A 68% reduction in plaque load was observed following IVIg-FUS treatment, compared to saline (Fig. 2K). Treatments with IVIg alone and FUS alone reduced plaque load by 57% and 40%, respectively, compared to saline (Fig. 2K). No difference was observed in the mean plaque size (*SI Appendix*, Fig. S2C).

Both IVIg alone and FUS alone have been independently reported to reduce Aβ plaque pathology and promote neurogenesis (8, 20–22, 35). As such, we next investigated whether an increase in neurogenesis in Tg animals could occur with FUS, IVIg, and IVIg-FUS treatments, in addition to a reduction in Aβ plaque pathology.

FUS Is Required for IVIg to Promote Hippocampal Neurogenesis. To evaluate the effects on neurogenesis, we quantified cells labeled with markers of proliferation (5-bromo-2-deoxyuridine, BrdU) and immature neurons (doublecortin, DCX) in all groups (Fig. 2 H and I, BrdU, red; DCX, green). In Tg mice, FUS treatment alone increased the number of BrdU$^+$ cells compared to saline (P < 0.05) and IVIg alone (P < 0.05) (Fig. 2L) (n = 5). IVIg-FUS treatments further increased the number of BrdU$^+$ cells compared to saline (P < 0.0001) and FUS alone (P < 0.01) (Fig. 2L). Notably, a threefold increase in proliferating cells (BrdU$^+$) with IVIg-FUS treatments was found compared to IVIg alone (P < 0.001) (Fig. 2L). IVIg-FUS also increased the number of posttreatment proliferating cells maturing toward a neuronal phenotype (BrdU$^+$/DCX$^+$) when compared to saline (P < 0.01), FUS (P < 0.05), and IVIg (P < 0.01) in Tg animals (Fig. 2M) (n = 5). The average number of BrdU$^+$/DCX$^+$ cells was three times higher in Tg mice treated with IVIg-FUS compared to IVIg alone (P < 0.01) (Fig. 2M). At the dosage of IVIg given intravenously, FUS was required for IVIg to have beneficial effects on hippocampal neurogenesis. These results contrast with the significant reduction in Aβ plaque load observed with IVIg alone. Indeed, with regards to hippocampal neurogenesis, IVIg alone did not increase cell proliferation (BrdU$^+$) nor cell differentiation (DCX$^+$). Further analysis supported the lack of correlation between Aβ plaque load and hippocampal cell proliferation in Tg animals (R^2 = 0.2) (*SI Appendix*, Fig. S2D). Therefore, in this experimental setting, decreasing Aβ load from a peripheral approach (i.e., with IVIg administration) is insufficient to promote neurogenesis.

We further demonstrated the necessity of FUS for IVIg-induced hippocampal neurogenesis, and the concept that this effect is independent of Aβ by using nTg mice, where Aβ pathology is lacking. In the hippocampus of nTg animals, the number of cells proliferating (BrdU$^+$) and differentiating in a neuronal phenotype (DCX$^+$) significantly increased only following IVIg-FUS treatments, compared to saline (P < 0.01), FUS (P < 0.05), and IVIg (P < 0.01) (Fig. 2 N and O).

Aside from the effects of IVIg on Aβ, IVIg has been characterized as an immunomodulatory agent (18, 44, 45). Because of the potential influence of IVIg on inflammatory cytokines, key modulators of neurogenesis (46), we next investigated whether treatments with IVIg and FUS impacted the inflammatory milieu in a different manner then IVIg alone in Tg mice.

IVIg-FUS Treatments Decrease Hippocampal TNF-α. Investigating the hippocampal inflammatory milieu was motivated by the finding that IVIg-FUS treatments increased neurogenesis by threefold compared to IVIg treatment alone in Tg mice, and despite comparable ability of IVIg alone and IVIg-FUS to reduce Aβ plaque pathology. Therefore, using an exploratory study design (47), we assessed the levels of CCTFs, which could be

responsible for the increase of hippocampal neurogenesis in Tg mice treated with IVIg, with and without FUS.

Using multiplex laser-bead ELISA, of the 36 CCTF studied, 14 had detectable levels in the hippocampal formation, with some effects of treatments being observed in Tg and nTg mice (Fig. 3 A and B and *SI Appendix*, Fig. S3). We focused on the comparative analyses of treatments within Tg mice, a relevant model of AD for the development of therapeutic approaches. Among these, only TNF-α and CCL5 responded differently to IVIg-FUS compared to IVIg-alone treatments in Tg mice (Fig. 3 A and B). The hippocampal levels of proinflammatory cytokine TNF-α were lowered with IVIg-FUS treatment compared to IVIg (Fig. 3A) (P < 0.05). In contrast, mice treated with IVIg-FUS had elevated levels of chemokine CCL5 in the hippocampus compared to IVIg alone (Fig. 3B) (P < 0.05).

Considering that IVIg was administered intravenously and has immunomodulatory effects, we also investigated the changes in CCTF levels in the blood. TNF-α levels in the serum were elevated in IVIg-FUS compared to IVIg treated Tg mice (Fig. 3C) (P < 0.05), in contrast with the results observed in the hippocampus (Fig. 3A). CCL5 levels in the serum of Tg animals treated with FUS and IVIg-FUS were significantly higher compared to those treated with saline and IVIg alone, respectively (Fig. 3D) (P < 0.05). Additional differences in CCTFs of IVIg-FUS–treated Tg animals include increased CCL4 (Fig. 3E) (P < 0.05) and decreased CCL7 (Fig. 3F) (P < 0.001), compared to IVIg treatment alone. IL-2 and granulocyte-macrophage colony-stimulating factor (GM-CSF) levels between IVIg-FUS and IVIg-treated Tg animals were not statistically different. Both IVIg-FUS and IVIg treatments appear to induce CCL4, IL-2, and GM-CSF compared to low and undetectable levels in absence of IVIg (Fig. 3 E, G, and H). In summary, the serum data show that in Tg mice, FUS treatments combined with IVIg, administered intravenously, differentially alters the blood levels of the CCTFs TNF-α, CCL4, -5, and -7 compared to IVIg alone (Fig. 3 C–F). Such differential alteration of blood CCTFs between IVIg-FUS and IVIg treatments in Tg mice was not observed for IL-2 and GM-CSF (Fig. 3 G and H).

Through the elucidation of CCTFs produced in response to IVIg-FUS and IVIg treatments in Tg mice, we also uncovered significant changes in CCTFs in control groups (e.g., in Tg mice in response to FUS alone and in treated nTg mice) (Fig. 3 and *SI Appendix*, Fig. S3). Specifically, in Tg mice injected with saline, FUS treatments increased CCL5 (Fig. 3D) and decreased IL-1α (*SI Appendix*, Fig. S3A), IL-2 (*SI Appendix*, Fig. S3B), IL-17 (*SI Appendix*, Fig. S3G), TGF-β1 (*SI Appendix*, Fig. S3J), and TGF-β2 (*SI Appendix*, Fig. S3K).

Taken together, these results highlight the profile of CCTFs in response to IVIg-FUS compared to IVIg in Tg mice centrally (FUS-targeted hippocampus; e.g., decrease in TNF-α) and in the periphery (serum, e.g., increase in TNF-α).

Discussion

For over 30 y, IVIg has been used in several neurological disorders as an efficient immunomodulator and antiinflammatory, reviewed in refs. 5 and 11. Yet, the mechanisms of action of IVIg are poorly understood. In the context of AD, antibodies contained in IVIg could exert their activities by: 1) Binding to a broad spectrum of aggregating and pathological forms of Aβ and tau; 2) binding to Aβ contained in the blood and promoting the efflux of Aβ from the brain (i.e., the "peripheral sink" hypothesis); 3) engaging immune-mediated responses involved in the clearance of Aβ; 4) attenuating cell-death pathway and protecting neurons against Aβ; and 5) acting as immunomodulators potentially through FcγRIIB and sialylated Fc.

It is possible that the efficacy of previous clinical trials using IVIg, administered peripherally, in mild to moderate AD was limited due to the poor access of IVIg to the brain (7, 13, 15, 48).

Dubey et al.

NEUROSCIENCE

These trials primarily relied on the immunomodulatory effects of IVIg in the periphery, with some central effects achieved at high dosages over several months that are likely to be transient (7, 13, 15, 48). As demonstrated here, transcranial FUS-BBB permeability increased the bioavailability of IVIg from the blood to the hippocampus, where it reached therapeutic efficacy at relatively low dosage given intravenously. For the use of IVIg in clinical trials, lowering the effective dose required for efficacy can lessen the burden on the availability of IVIg as a natural resource, as it is reliant on human blood donors and it is in high demand for treating several neurological diseases (17, 18).

We postulated that IVIg, combined with noninvasive FUS-mediated therapeutic delivery to the hippocampus (27), could enhance treatment efficacy. Over the last decade, safe acoustic parameters of FUS-induced BBB permeability have been established in animal models and in humans, as recently reviewed in Meng et al. (27). In animal models, the use of safe parameters was shown to prevent or minimize red blood cell extravasation (27). Blood-borne molecules can briefly enter the brain and be cleared within hours [i.e., albumin (49)] to 4 d [i.e., IgG and IgM (20)]. Inflammation has been reported to occur acutely after FUS in some but not all conditions (50–54). At longer-term post-FUS, evidence suggests putative beneficial effects of albumin, IgG, and IgM in reducing AD pathology and establishing a proregenerative milieu (20–22, 27, 55, 56). To date, in animal models of AD, the long-term effects of single and repeated FUS treatments—even without the addition of a therapeutic—have led to the reduction of Aβ and tau pathologies, and to the promotion of hippocampal neurogenesis, parenchymal nerve growth factor content, TrkA-related survival signaling pathways, and cognitive functions (3, 21, 22, 33, 57–62). When acoustic settings are selected to avoid edema and microbleeds, the restoration of the BBB post-FUS occurs between 6 and 24 h in animal models, and in patients with AD and amyotrophic lateral sclerosis (20, 24–29, 32). Recent clinical trials have described FUS-induced BBB permeability as safe, reproducible, and transient in people with AD and amyotrophic lateral sclerosis (28–30, 63). Here, we provide further evidence that two FUS treatments by themselves reduce Aβ plaque pathology, and we discovered that combined with IVIg, FUS can further enhance treatment efficacy in reducing the proinflammatory cytokine TNF-α and promoting neurogenesis in the hippocampal formation of a Tg mouse model of AD.

Our bioavailability data demonstrate that one administration of 0.4 g IVIg/kg (12 mg per Tg mouse, intravenously) resulted in 489 ng IVIg/mg of protein in FUS-targeted hippocampi, compared to undetectable levels in non-FUS–targeted hippocampi, at 4 h posttreatment. In these conditions, FUS allowed on average 0.09% of the dose of IVIg injected intravenously to enter the hippocampus. A study by St-Amour et al. (16) demonstrated that of 1.5 g IVIg/kg (25 mg per mouse, intraperitoneally) in C57BL/6 mice delivered 12.5 ng IVIg/mg of protein to the hippocampus, the equivalent of 0.0017% of the injected dose. As such, FUS delivery translates in an approximate 39-fold greater delivery to the hippocampus (489 ng/mg vs. 12.5 ng/mg) by using less than half the dose administered peripherally (intraperitoneally) (12 mg vs. 25 mg). Furthermore, it remains possible that we did not capture the maximal levels of IVIg levels reaching FUS-targeted hippocampi post-FUS for three main reasons. First, the timeline of FUS-induced BBB permeability (24, 26, 64) could have led to the accumulation of IVIg in the targeted hippocampi at a time-point that was not captured between 4 and 24 h. Second, the saline perfusion, aimed to remove IVIg still circulating in the blood and avoid confounding results, may have also cleared some of the IVIg from the hippocampal tissue. Third, IVIg was delivered at two defined FUS spots to the hippocampus, hence underestimating the amount of IVI in nanograms/milligram delivered at each FUS spot by measuring IVIg

in total hippocampal tissue. Increasing the number of FUS spots to target the entire hippocampal formation would be of interest to address this potential limitation in the measurement of bioavailability. The clearance of IVIg from the FUS-targeted hippocampi at 7 d posttreatment is in line with the previously established half-life of IVIg in the hippocampus by St-Amour et al. (16) (i.e., 140 h [5.8 d]).

Two-photon microscopy analyses demonstrated that, in response to FUS, amyloid-coated vessels in 6- to 8-mo-old Tg mice have reduced permeability and a limited capacity for change in diameter compared to measurements observed in nTg mice (65). In contrast, the levels of GAD enhancement, visualized by MRI following FUS-induced BBB permeability, are not significantly different between Tg and nTg mice (3, 20, 22, 32). Congruent with these data, the amount of therapeutic—that is, IVIg (present study) and D3 (3)—found in targeted brain areas post-FUS is similar between Tg and nTg mice. In patients with AD, repeated FUS-induced BBB modulations has been reported to be safe, with predictable detection of GAD enhancement to visualize the increase in BBB permeability within few minutes, and its restoration within 24 h (29, 30).

The pharmacokinetics of IVIg-FUS delivery in the present study have limitations. For example, each FUS spot has variability in response to BBB permeability in time and space. The current experimental design did not account for these variables; the resected tissue for bioavailability analysis was taken at the same time point for all animals and included larger volume of tissue relative to the two FUS spots targeted for IVIg delivery. These characteristics are bound to introduce greater variability in IVIg measurements delivered by FUS compared to a traditional pharmacokinetics evaluation of a compound homogeneously crossing the BBB. The increased IVIg delivery by FUS and clearance by 7 d supported the notion of testing the effects of two weekly IVIg-FUS bilateral treatments on Aβ plaque pathology and neurogenesis.

With regards to neurogenesis, a previous study reported that 8 mo of IVIg administration at a high dose (1.0 g/kg/wk, intravenously; cumulative dose of 32 g/kg) increased the number of immature neurons (DCX+) in the hippocampus of APP/PS1 mice (10). Here, we aimed to improve treatment efficacy on neurogenesis by delivering IVIg to the hippocampus with FUS, and identifying whether a putative increase in DCX+ cells comes from newly proliferating cells or the enhanced survival of immature neurons. Considering the data obtained in the bioavailability study, IVIg was administered at 0.4 g/kg (intravenously), weekly for 2 wk, with and without FUS-targeting to the hippocampi. The results clearly show that two IVIg-FUS treatments, each delivering an estimated 489 ng/mg of IVIg to the hippocampus—representing ~0.09% of the injected dose—were sufficient to reach an effective concentration to promote neurogenesis. Indeed, two treatments of IVIg-FUS, and not IVIg without FUS, increased the proliferation and survival of newborn cells differentiating into immature neurons. Hippocampal progenitors, contributing to adult hippocampal neurogenesis, play a critical role in pattern separation, cognitive function, and long-term memory (66–68). Compared to Puli et al. (10), IVI-FUS treatments reduced the cumulative effective dose of IVIg from 32 g/kg (1 g/kg/wk, intravenously) to 0.8 g/kg (0.4 g/kg/wk, intravenously) to promote neurogenesis. In Puli et al. (10), the 8-mo IVIg treatment increased the number of DCX+ cells by less than twofold compared to saline. Here, two IVIg-FUS treatments quadrupled the number of BrdU/DCX+ cells in the hippocampus compared to saline. FUS alone had been previously characterized as increasing adult hippocampal neurogenesis through cell proliferation, maturation, and survival (i.e., augmenting the numbers of BrdU+, DCX+, and BrdU/NeuN+ cells) (21–23, 69). Here we found that the main effects of IVIg-FUS are in augmenting cell proliferation (BrdU+), maintaining differentiation and survival

of newborn neurons (BrdU/DCX$^+$). The levels of hippocampal neurogenesis induced by IVIg-FUS were 4-, 3-, and 1.5-fold higher than in Tg mice treated with saline, IVIg alone, and FUS alone, respectively. This is remarkable considering that exercise, one of the most potent modulators of neurogenesis, does not significantly increase hippocampal neurogenesis in Tg mice running between 3 and 4 mo of age (39), which would represent a similar timeline to the present study. Furthermore, running typically results in maximal increases in hippocampal neurogenesis by two- to threefold (70) (i.e., below the fourfold increase observed here). In light of recent clinical trials using FUS to modulate the BBB in patients with AD (29, 30), elucidating the effects of FUS alone and combined with therapeutics in the hippocampus is critical. Adult neurogenesis declines rapidly with age and AD (71–73), and we here provide evidence on the capacity of IVIg to potentiate hippocampal neurogenesis in combination with FUS.

The beneficial effects of IVIg-FUS treatments on neurogenesis could not be explained solely by the reduction of Aβ levels in Tg mice, as they were also observed in nTg animals where Aβ pathology is nonexistent. Therefore, the promotion of neurogenesis by IVIg-FUS does not require Aβ-related mechanisms. IVIg has been previously reported to increase synaptic function without reducing Aβ pathology in Tg2576 mice, providing another example of the effects of IVIg on neuronal plasticity independently of Aβ reduction (74). Taken together, our data suggest that the beneficial effects of IVIg-FUS on neurogenesis, and IVIg on Aβ plaque pathology—found to be efficient with or without FUS—could be mediated by distinct modulation of central (hippocampus) and peripheral (blood) inflammation, respectively. Previous work has shown that repeated IVIg administration does not increase anti-human IgG response in mice (8). Instead, IVIg alters the inflammatory environment (11). Therefore, the changes of peripheral (serum) CCTFs seen in our work is attributed to immunomodulation effect of IVIg, which can contribute to reducing Aβ plaque pathology as observed in IVIg treatments alone. Conversely, neurogenesis is most likely to be modulated directly in the hippocampus, where IVIg and FUS combined alter the microenvironment. Notably, we found that IVIg-FUS treatments decreased the proinflammatory TNF-α, known to inhibit adult neurogenesis (46). TNF-α can also influence Aβ pathologies and cognitive deficits in murine models of AD (75, 76).

Our data reveal that IVIg-FUS decreased TNF-α and increased CCL5 in the hippocampus of Tg mice compared to IVIg treatment alone. In addition, IVIg-FUS therapy increased serum TNF-α, CCL4, and CCL5, and decreased serum CCL7 in Tg animals. It is clear, the factor responsible for increases in CCL4, IL-2, and GM-CSF in the serum is IVIg, and not FUS. CCL4, CCL5, and CCL7 are chemokines that regulate monocyte and T cell entry into the brain and, along with TNF-α, can be modulated by IVIg (77–80). Furthermore, CCL5, which is increased both in the serum and the hippocampus, has been associated with cognitive benefits of exercise and is lowered in the serum of AD patients (80–82). Therefore, IVIg-FUS may modulate the chemotactic signaling and transmigration of monocytes and T cells by reversing the lowered levels of serum CCL5 in Tg animals.

IVIg-FUS also decreased hippocampal TNF-α and increased serum TNF-α in Tg animals. Our data indicate that combined IVIg-FUS treatments modify the equilibrium of TNF-α centrally and peripherally. The mechanisms leading to reduced TNF-α in the hippocampus and increased TNF-α in the serum remain to be identified, including potential exchanges of TNF-α through the BBB (83). Elevated serum levels of TNF-α (>100 pg/mL) have been shown to induce proinflammatory signaling in the blood and brain (84). IVIg-FUS increased TNF-α levels in the serum to 50 pg/mL, which did not globally transform the hippocampal milieu as proinflammatory. Other studies have shown that elevated hippocampal TNF-α promotes Aβ production (85–87) and reduces neurogenesis (88). IVIg injected into the brain of APP/PS1 mice reduced the relative gene expression of TNF-α (89). Here, IVIg-FUS treatments decreased hippocampal Aβ plaque load, similar to IVIg treatments alone. In contrast, delivering IVIg to the hippocampus noninvasively with FUS led to additional beneficial effects known to influence cognitive outcomes (e.g., decreasing TNF-α and promoting neurogenesis). For example, IVIg-FUS could counteract the deleterious impact of TNF-α on neuronal excitability underlying cognitive dysfunction in Tg mice (90, 91). Augmenting the dose of IVIg to the brain with FUS could improve novel object recognition memory and reduce anxiety-like behavior, as seen in 3xTg-AD mice following chronic IVIg delivery at a high dose of 1.5 g/kg (9 to 27 intraperitoneal injections) (8). And finally, it has been demonstrated that inducing a greater than or equal to twofold increase in proliferation/survival of hippocampal progenitor cells in Tg mice can be accompanied by enhanced cognitive function (39). Therefore, the increase in the bioavailability of IVIg to the hippocampus by FUS, the reduction of TNF-α and fourfold increase in neurogenesis, strongly suggest that this therapeutic approach could improve cognitive function.

In summary, we found that at a relatively low dosage, IVIg, administered intravenously and combined with FUS-targeted BBB permeability, delivered sufficient amount of IVIg to the hippocampus to decrease TNF-α and promote neurogenesis, while also harnessing the effects of IVIg alone (intravenously) to reduce Aβ plaque pathology and modulate serum CCTFs. In contrast, without FUS, IVIg administered intravenously did not significantly cross the BBB, and while it reduced Aβ pathology, it did not increase hippocampal neurogenesis nor reduce TNF-α in the brain. Given the potential of FUS to reversibly modulate the BBB in patients with AD (29, 30), our results suggest an approach for the use of IVIg in AD and other neurological diseases, where the BBB poses a limitation for effective therapeutic delivery and efficacy.

Materials and Methods

All data discussed is included in the main text and *SI Appendix*, and was generated as per methodology described here.

Animals. The TgCRND8 (Tg) mouse model of amyloidosis overexpresses the human amyloid precursor protein (APP) 695 containing the KM670/671NL and V717F mutations under control of the hamster prion promoter. By 90 d of age, amyloid plaque deposits in the forebrain are evident (36, 92). A total of 107 Tg and 116 nTg animals, sex-balanced and age matched, were used for the bioavailability and repeated efficacy studies. Forty-eight Tg and nTg were used for the bioavailability study, starting at the age of 97 to 128 d and killed at four different time points assessed in both genotypes (4 h, 24 h, 7 d, 14 d; *n* = 6 per group) for IVIg quantification. Fifty-nine Tg and 68 nTg were used in the efficacy study at the age of 104 ± 2 d for treatments and killed at 21 d posttreatment for both immunohistochemistry and biochemical tissue processing. All animals were bred and housed at Sunnybrook Research Institute. All experiments were carried out in accordance with the guidelines provided by the Animal Care Committee at Sunnybrook Research Institute and the Canadian Council on Animal Care and Animals for Research Act of Ontario.

MRI-Guided FUS for Targeted BBB Permeability. On the day of the experiment, animals underwent anesthesia with isoflurane, followed by depilation of the head, and tail vein catheterization for drug delivery. While under anesthesia, animals were placed in dorsal recumbancy on a positioning sled, which was placed inside the 7T MRI (BioSpin 7030; Bruker) for T2w and T1w image acquisition (21, 22, 93, 94). The sled was fitted on the FUS system with the animal's head resting in a degassed water bath and positioned above a spherical FUS transducer (1.68 MHz, 75-mm diameter and 60-mm radius of curvature). The transducer was built-in with a small custom PVDF hydrophone in the center of the transmit transducer (94, 95). The acquired T2w image was registered with the FUS transducer for bilateral hippocampal targeting in the *x*, *y*, and *z* plane. Once the brain regions to target were

NEUROSCIENCE

identified, Definity microbubbles (0.02 mL/kg; Lantheus Medical Imaging) were injected intravenously at the onset of sonication for BBB permeabilization (1-Hz burst repetition frequency, 10-ms bursts, 120 s in total). With the use of a feedback controller, the sonications were controlled and allowed for consistent BBB permeabilization irrespective of skull thickness and vasculature variability between subjects (94, 95). Following ultrasound sonication, GAD-based MRI contrast agent, GAD (Omniscan 0.5 mM/mL, GE Healthcare) and IVIg where applicable (Gammagard Liquid 10%, Baxter) were injected at the dose of 0.2 mL/kg and 0.4 g/kg, respectively. Post-sonication, animals were returned to the MRI for T1w image acquisition to confirm the BBB permeabilization through GAD entry into the brain parenchyma, as visualized as signal hyperintensity or enhancement.

Bioavailability study. Using the FUS parameters listed above, nTg and Tg animals were administered 0.4 g/kg IVIg intravenously and the left side of the brain was targeted by FUS, under MRI guidance. Specifically, two FUS spots were used per brain region, namely the left hippocampus and cortex, while the right side of the brain was used as the internal control.

Treatment efficacy study. Tg and nTg animals were divided into one of four treatment groups: Saline, IVIg, FUS, or IVIg-FUS. IVIg-FUS animals were treated as outlined above. Four hippocampal targets were used, two in each dorsal hippocampus. Animals treated with only IVIg or saline were anesthetized, depilated, and injected with the respective treatment through a tail vein catheter without undergoing MRI or FUS sonication. Posttreatment, all animals were injected with BrdU (50 mg/kg) for 4 consecutive days followed by a second treatment on day 8. Matlab software (Mathworks) was used to quantify enhancement via measuring pixel intensity of a 2×2-mm area within the region of interest (four FUS focal spots). This was done using GAD-enhanced T1w MRI images acquired after FUS treatment. The intensity was averaged over the four spots per animal and compared between Tg and nTg to ensure consistency in BBB permeabilization between genotypes.

Biochemical Analyses. The animals were anesthetized using an intraperitoneal injection of ketamine (200 mg/kg) and xylazine (25 mg/kg), blood was collected from the right ventricle for serum collection followed by intracardial perfusion (left ventricle) with 0.9% saline. The brain tissue was rapidly dissected and flash frozen in liquid nitrogen. The serum samples and dissected brain tissue was stored at -80 °C until further use.

Human IgG ELISA. For bioavailability study, the snap-frozen hippocampus and cortex tissue was homogenized in lysis buffer and lysates were analyzed using species-specific ELISA using IgG Fc-specific antibodies for capture and the corresponding HRP-conjugated antibodies for detection (Jackson ImmunoResearch Laboratories).

CCTFs. Half of the homogenized hippocampal tissue was sent for analysis to Eve Technologies for a multiplexing laser bead assay (Mouse Cytokine/Chemokine Array 31-Plex and TGF-β 3-plex) for an exploratory study design. The following 36 analytes were targeted: CCL11 (Eotaxin), G-CSF, GM-CSF, M-CSF, IFN-γ, IL-1α, IL-1β, IL-2, IL-3, IL-4, IL-5, IL-6, IL-7, IL-9, IL-10, IL-12 (p40), IL-12 (p70), IL-13, IL-15, IL-17A, CXCL10 (IP10), CXCL1 (KC), LIF, LIX, MCP1 (CCL2), CXCL9 (MIG), CCL3 (MIP1a), CCL4 (MIP1b), CXCL2 (MIP2), CCL5 (RANTES), TNF-α, VEGF, LIX, TGF-β1, TGF-β2 and TGF-β3. The experimental conditions and the technology itself minimize potential nonspecific binding and detection, including from endogenous biotin. Specifically, the target analyte is detected by a capture antibody attached to a fluorescent bead and a detection antibody attached to the streptavidin-phycoerythrin reporter. Furthermore, several analytes were undetectable (i.e., G-CSF, M-CSF, IFN-γ, IL-3, IL-5, IL-6, IL-12 (p40), LIX, LIF, and MIP-1b), confirming the lack of significant nonspecific detection. Results are reported in picograms per milliliter for analytes that were above baseline.

Serum levels of 20 CCTF factors were evaluated by using a multiple analyte detection system (FlowCytomix; eBioscience) as per kit instructions. The factors measured were: IL-1α, IL-2, IL-4, IL-5, IL-6, IL-10, IL-13, IL-17 A/F, IL-18, IL-23, CXCL-1 (KC), GM-CSF, MCP-1 (CCL-2), MCP-3 (CCL-7), CCL-4 (MIP-1b), CCL-3 (MIP-1a), CCL-5 (RANTES), CXCL-10 (IP-10), IFN-γ, and TNF-α. Flow cytometric analysis was performed using FACS Calibur (BD Biosciences) and detected results were reported in picograms per milliliter

Immunohistochemistry. All animals were killed for tissue collection 21 d after the treatment paradigm began. Animals were deeply anesthetized using an intraperitoneal injection of ketamine (200 mg/kg) and xylazine (25 mg/kg), followed by intracardial perfusion with 0.9% saline and 4% paraformaldehyde (PFA). Whole brains were collected and postfixed in 4% PFA overnight before transfer to 30% sucrose at 4 °C and kept until the brains sank to the bottom. Brains were cut into serial 40-μm-thick coronal sections using a sliding microtome (Leica). A systematic sampling method was used to select

sections at an interval of 12 throughout the hippocampus (from 0.94 mm to 2.92 mm posterior of Bregma) for immunohistochemistry.

Sections used for Aβ plaques were first incubated in a blocking solution (1% bovine serum, 2% donkey serum and 0.35% Triton-X100 in PBS) for 1 h. Following blocking, sections were incubated in mouse 6F3D antibody targeting human Aβ (1:200; Dako North American) overnight at 4 °C. Subsequently, sections were washed in PBS and incubated in donkey anti-mouse-Cy3 and donkey anti-goat-Cy5 (1:200; Jackson Immuno-Research Laboratories) for 1 h, washed in PBS, and mounted on slides.

Confocal Imaging and Analysis. For IVIg staining, sections were incubated in 3% hydrogen peroxide for 10 min, rinsed, and incubated overnight in biotinylated primary antibody against human IgG (1:100; Santa Cruz, Product SC2775, Lot G0212). Following PBS rinse, sections were incubated in streptavidin-conjugated HRP (1:1,000; Jackson ImmunoResearch Laboratories, Product 016030084, Lot 82330) and 3,3-diaminobenzidine (DAB kit; Sigma). Sections were mounted on slides, dehydrated by serial treatment in ethanol and propanol solutions, and coverslipped.

For BrdU and DCX and staining, sections were incubated in blocking serum (10% donkey serum and 0.25% Triton-X100 in PBS) for 1 h. After blocking, sections were incubated with a goat anti-mouse DCX antibody (1:200; Santa Cruz) for 48 h. This was followed by washes in PBS and incubation in donkey anti-goat Alexa 488 (1:200; Jackson ImmunoResearch Laboratories) for 2 h. Sections were subsequently rinsed and treated with 2N HCl (37 °C, 35 min) for antigen retrieval, followed by neutralization through treatment with 0.1 M borate buffer (pH 8.5). Postneutralization, sections were rinsed with PBS and incubated overnight in rat anti-mouse BrdU antibody (1:400; AbD Serotec). The next day, sections were rinsed and incubated in donkey anti-rat Cy3 (1:200) for 1 h. This was followed by PBS rinses and sections were mounted on slides.

For IVIg immunoreactivity in the bilateral hippocampus, brightfield virtual montages were acquired using a 20$\times$ objective (0.8 NA) on a Zeiss Axioplan 2 microscope and the 2D Virtual Slice module of Stereo Investigator 10 (MBF BioScience). For the rest of the immunofluorescence imaging, a spinning disk confocal microscope (CSU-W1; Yokogawa Electric, Zeiss Axio Observer.Z1, Carl Zeiss) was used to acquire z-stack images of the entire hippocampus. Using the tiling feature of the Zen 2012 software v1.1.2 (Carl Zeiss), a composite image of the hippocampus was created in three dimensions. For Aβ plaque immunoreactivity quantification, images were acquired using a 20$\times$ objective (0.8 NA) in the Cy3 channels and a maximum intensity projection image was generated for analysis in the ImageJ software. Using the particle analysis feature of ImageJ, the number and area of plaques in the entire hippocampus was calculated.

For BrdU and DCX cell quantification, images were acquired at 63$\times$ (1.40 NA) in the Cy3 and Cy2 channels, respectively. An observer blinded to treatment using the Zen software carried out the cell counting for BrdU$^+$ cells and BrdU/DCX$^+$ cells. The total number of BrdU$^+$ and BrdU/DCX$^+$ was multiplied by the sampling interval value (1 in 12, three to four sections per animal) in order to estimate of the total number of cells in the entire hippocampus per animal.

Statistical Analysis. Statistical analysis was done in GraphPad Prism 5 and 8. In bar graphs, data are represented as mean + SD. GAD enhancements between Tg and nTg were compared with unpaired t tests, and no statistical significance was noted. For bioavailability studies, Wilcoxon matched-pairs signed rank one-tail tests were performed, under the assumption that greater levels of IVIg will be found in FUS-treated regions. Significant differences were noted at $P < 0.05$. For the efficacy of two treatments (saline, IVIg, FUS, IVIg-FUS), one-way ANOVA was used to compare all treatment groups to each other for IVIg immunoreactivity, Aβ total plaque number, mean size and surface area, BrdU$^+$, and BrdU/DCX$^+$ cells. A Newman–Keuls method was applied as post hoc analysis and differences were significant at $P < 0.05$. For analysis of CCTFs in the brain and serum, we asked the question of how IVIg-FUS treatment compared to IVIg alone and FUS treatment compared with saline alone. Therefore, unpaired t tests were carried out for each comparison and significant differences reported at $P < 0.05$. For the serum analysis of TNF-α, CCL4, IL-2, and GM-CSF, differences between treatment groups were analyzed using nonparametric Mann–Whitney test (due to a high proportion of zero values) and significance set at $P < 0.05$.

Note Added in Proof. A comprehensive review was published after the current manuscript was accepted (96).

Data Availability. All study data are included in the article and *SI Appendix*.

Dubey et al.

www.manaraa.com

1. Alzheimer's Association, Alzheimer's disease facts and figures. *Alzheimers Dement.* **14**, 367–429 (2018).
2. N. Baazaoui, K. Iqbal, A novel therapeutic approach to treat Alzheimer's disease by neurotrophic support during the period of synaptic compensation. *J. Alzheimers Dis.* **62**, 1211–1218 (2018).
3. K. Xhima et al., Focused ultrasound delivery of a selective TrkA agonist rescues cholinergic function in a mouse model of Alzheimer's disease. *Sci. Adv.* **6**, eaax6646 (2020).
4. L. Hromadkova, S. V. Ovsepian, Tau-reactive endogenous antibodies: Origin, functionality, and implications for the pathophysiology of Alzheimer's disease. *J. Immunol. Res.* **2019**, 7406810 (2019).
5. A. Manolopoulos et al., Intravenous immunoglobulin for patients with Alzheimer's disease: A systematic review and meta-analysis. *Am. J. Alzheimers Dis. Other Demen.* **34**, 281–289 (2019).
6. J. Magga et al., Human intravenous immunoglobulin provides protection against Aβ toxicity by multiple mechanisms in a mouse model of Alzheimer's disease. *J. Neuroinflammation* **7**, 90 (2010).
7. R. Dodel et al., Intravenous immunoglobulin for treatment of mild-to-moderate Alzheimer's disease: A phase 2, randomised, double-blind, placebo-controlled, dose-finding trial. *Lancet Neurol.* **12**, 233–243 (2013).
8. I. St-Amour et al., IVIg protects the 3xTg-AD mouse model of Alzheimer's disease from memory deficit and Aβ pathology. *J. Neuroinflammation* **11**, 54 (2014).
9. I. St-Amour, F. Cicchetti, F. Calon, Immunotherapies in Alzheimer's disease: Too much, too little, too late or off-target? *Acta Neuropathol.* **131**, 481–504 (2016).
10. L. Puli et al., Effects of human intravenous immunoglobulin on amyloid pathology and neuroinflammation in a mouse model of Alzheimer's disease. *J. Neuroinflammation* **9**, 105 (2012).
11. J. D. Lünemann, F. Nimmerjahn, M. C. Dalakas, Intravenous immunoglobulin in neurology—Mode of action and clinical efficacy. *Nat. Rev. Neurol.* **11**, 80–89 (2015).
12. S. E. Counts, S. E. Perez, B. He, E. J. Mufson, Intravenous immunoglobulin reduces tau pathology and preserves neuroplastic gene expression in the 3xTg mouse model of Alzheimer's disease. *Curr. Alzheimer Res.* **11**, 655–663 (2014).
13. N. R. Relkin et al.; Alzheimer's Disease Cooperative Study, A phase 3 trial of IV immunoglobulin for Alzheimer disease. *Neurology* **88**, 1768–1775 (2017).
14. N. Relkin, Clinical trials of intravenous immunoglobulin for Alzheimer's disease. *J. Clin. Immunol.* **34** (suppl. 1), S74–S79 (2014).
15. S. Kile et al., IVIG treatment of mild cognitive impairment due to Alzheimer's disease: A randomised double-blinded exploratory study of the effect on brain atrophy, cognition and conversion to dementia. *J. Neurol. Neurosurg. Psychiatry* **88**, 106–112 (2017).
16. I. St-Amour et al., Brain bioavailability of human intravenous immunoglobulin and its transport through the murine blood-brain barrier. *J. Cereb. Blood Flow Metab.* **33**, 1983–1992 (2013).
17. D. A. Loeffler, Should development of Alzheimer's disease-specific intravenous immunoglobulin be considered? *J. Neuroinflammation* **11**, 198 (2014).
18. E. E. Perez et al., Update on the use of immunoglobulin in human disease: A review of evidence. *J. Allergy Clin. Immunol.* **139**, S1–S46 (2017).
19. A. W. Zuercher, R. Spirig, A. Baz Morelli, T. Rowe, F. Käsermann, Next-generation Fc receptor-targeting biologics for autoimmune diseases. *Autoimmun. Rev.* **18**, 102366 (2019).
20. J. F. Jordão et al., Amyloid-β plaque reduction, endogenous antibody delivery and glial activation by brain-targeted, transcranial focused ultrasound. *Exp. Neurol.* **248**, 16–29 (2013).
21. T. Scarcelli et al., Stimulation of hippocampal neurogenesis by transcranial focused ultrasound and microbubbles in adult mice. *Brain Stimul.* **7**, 304–307 (2014).
22. A. Burgess et al., Alzheimer disease in a mouse model: MR imaging-guided focused ultrasound targeted to the hippocampus opens the blood-brain barrier and improves pathologic abnormalities and behavior. *Radiology* **273**, 736–745 (2014).
23. J. Shin et al., Focused ultrasound-induced blood-brain barrier opening improves adult hippocampal neurogenesis and cognitive function in a cholinergic degeneration dementia rat model. *Alzheimers Res. Ther.* **11**, 110 (2019).
24. K. Hynynen, N. McDannold, N. Vykhodtseva, F. A. Jolesz, Noninvasive MR imaging-guided focal opening of the blood-brain barrier in rabbits. *Radiology* **220**, 640–646 (2001).
25. M. A. O'Reilly, O. Hough, K. Hynynen, Blood-brain barrier closure time after controlled ultrasound-induced opening is independent of opening volume. *J. Ultrasound Med.* **36**, 475–483 (2017).
26. N. McDannold, N. Vykhodtseva, K. Hynynen, Blood-brain barrier disruption induced by focused ultrasound and circulating preformed microbubbles appears to be characterized by the mechanical index. *Ultrasound Med. Biol.* **34**, 834–840 (2008).
27. Y. Meng et al., Safety and efficacy of focused ultrasound induced blood-brain barrier opening, an integrative review of animal and human studies. *J. Control. Release* **309**, 25–36 (2019).
28. A. Abrahao et al., First-in-human trial of blood-brain barrier opening in amyotrophic lateral sclerosis using MR-guided focused ultrasound. *Nat. Commun.* **10**, 4373 (2019).
29. N. Lipsman et al., Blood-brain barrier opening in Alzheimer's disease using MR-guided focused ultrasound. *Nat. Commun.* **9**, 2336 (2018).
30. A. R. Rezai et al., Noninvasive hippocampal blood-brain barrier opening in Alzheimer's disease with focused ultrasound. *Proc. Natl. Acad. Sci. U.S.A.* **117**, 9180–9182 (2020).
31. S. B. Raymond et al., Ultrasound enhanced delivery of molecular imaging and therapeutic agents in Alzheimer's disease mouse models. *PLoS One* **3**, e2175 (2008).
32. J. F. Jordão et al., Antibodies targeted to the brain with image-guided focused ultrasound reduces amyloid-beta plaque load in the TgCRND8 mouse model of Alzheimer's disease. *PLoS One* **5**, e10549 (2010).
33. R. M. Nisbet et al., Combined effects of scanning ultrasound and a tau-specific single chain antibody in a tau transgenic mouse model. *Brain* **140**, 1220–1230 (2017).
34. T. Alecou, M. Giannakou, C. Damianou, Amyloid β plaque reduction with antibodies crossing the blood-brain barrier, which was opened in 3 sessions of focused ultrasound in a rabbit model. *J. Ultrasound Med.* **36**, 2257–2270 (2017).
35. M. Yu et al., Selective impairment of hippocampus and posterior hub areas in Alzheimer's disease: An MEG-based multiplex network study. *Brain* **140**, 1466–1485 (2017).
36. M. A. Chishti et al., Early-onset amyloid deposition and cognitive deficits in transgenic mice expressing a double mutant form of amyloid precursor protein 695. *J. Biol. Chem.* **276**, 21562–21570 (2001).
37. S. Dudal et al., Inflammation occurs early during the Abeta deposition process in TgCRND8 mice. *Neurobiol. Aging* **25**, 861–871 (2004).
38. C. Cavanagh et al., βCTF-correlated burst of hippocampal TNFα occurs at a very early, pre-plaque stage in the TgCRND8 mouse model of Alzheimer's disease. *J. Alzheimers Dis.* **36**, 233–238 (2013).
39. E. Maliszewska-Cyna, K. Xhima, I. Aubert, A comparative study evaluating the impact of physical exercise on disease progression in a mouse model of Alzheimer's disease. *J. Alzheimers Dis.* **53**, 243–257 (2016).
40. B. M. Francis et al., Object recognition memory and BDNF expression are reduced in young TgCRND8 mice. *Neurobiol. Aging* **33**, 555–563 (2012).
41. A. Bellucci et al., Cholinergic dysfunction, neuronal damage and axonal loss in TgCRND8 mice. *Neurobiol. Dis.* **23**, 260–272 (2006).
42. S. Krantic et al., Hippocampal GABAergic neurons are susceptible to amyloid-β toxicity in vitro and are decreased in number in the Alzheimer's disease TgCRND8 mouse model. *J. Alzheimers Dis.* **29**, 293–308 (2012).
43. S. Krantic, Editorial: From current diagnostic tools and therapeutics for Alzheimer's disease towards earlier diagnostic markers and treatment targets. *Curr. Alzheimer Res.* **14**, 2–5 (2017).
44. C. João, V. S. Negi, M. D. Kazatchkine, J. Bayry, S. V. Kaveri, Passive serum therapy to immunomodulation by IVIg: A fascinating journey of antibodies. *J. Immunol.* **200**, 1957–1963 (2018).
45. W. A. Sewell, S. Jolles, Immunomodulatory action of intravenous immunoglobulin. *Immunology* **107**, 387–393 (2002).
46. A. Borsini, P. A. Zunszain, S. Thuret, C. M. Pariante, The role of inflammatory cytokines as key modulators of neurogenesis. *Trends Neurosci.* **38**, 145–157 (2015).
47. J. Kimmelman, J. S. Mogil, U. Dirnagl, Distinguishing between exploratory and confirmatory preclinical research will improve translation. *PLoS Biol.* **12**, e1001863 (2014).
48. R. Dodel et al., Intravenous immunoglobulins as a treatment for Alzheimer's disease: Rationale and current evidence. *Drugs* **70**, 513–528 (2010).
49. A. Alonso, E. Reinz, M. Fatar, M. G. Hennerici, S. Meairs, Clearance of albumin following ultrasound-induced blood-brain barrier opening is mediated by glial but not neuronal cells. *Brain Res.* **1411**, 9–16 (2011).
50. Z. I. Kovacs et al., MRI and histological evaluation of pulsed focused ultrasound and microbubbles treatment effects in the brain. *Theranostics* **8**, 4837–4855 (2018).
51. Z. I. Kovacs et al., Disrupting the blood-brain barrier by focused ultrasound induces sterile inflammation. *Proc. Natl. Acad. Sci. U.S.A.* **114**, E75–E84 (2017).
52. D. McMahon, C. Poon, K. Hynynen, Evaluating the safety profile of focused ultrasound and microbubble-mediated treatments to increase blood-brain barrier permeability. *Expert Opin. Drug Deliv.* **16**, 129–142 (2019).
53. D. McMahon, R. Bendayan, K. Hynynen, Acute effects of focused ultrasound-induced increases in blood-brain barrier permeability on rat microvascular transcriptome. *Sci. Rep.* **7**, 45657 (2017).
54. D. McMahon, K. Hynynen, Acute inflammatory response following increased blood-brain barrier permeability induced by focused ultrasound is dependent on microbubble dose. *Theranostics* **7**, 3989–4000 (2017).
55. G. Leinenga, J. Götz, Scanning ultrasound removes amyloid-β and restores memory in an Alzheimer's disease mouse model. *Sci. Transl. Med.* **7**, 278ra33 (2015).
56. J. Silburt, N. Lipsman, I. Aubert, Disrupting the blood-brain barrier with focused ultrasound: Perspectives on inflammation and regeneration. *Proc. Natl. Acad. Sci. U.S.A.* **114**, E6735–E6736 (2017).
57. R. Pandit, G. Leinenga, J. Götz, Repeated ultrasound treatment of tau transgenic mice clears neuronal tau by autophagy and improves behavioral functions. *Theranostics* **9**, 3754–3767 (2019).

NEUROSCIENCE

Dubey et al.

www.manaraa.com

58. P. W. Janowicz, G. Leinenga, J. Götz, R. M. Nisbet, Ultrasound-mediated blood-brain barrier opening enhances delivery of therapeutically relevant formats of a tau-specific antibody. *Sci. Rep.* **9**, 9255 (2019).

59. G. Leinenga, W. K. Koh, J. Götz, Scanning ultrasound in the absence of blood-brain barrier opening is not sufficient to clear β-amyloid plaques in the APP23 mouse model of Alzheimer's disease. *Brain Res. Bull.* **153**, 8–14 (2019).

60. G. Leinenga, J. Götz, Safety and efficacy of scanning ultrasound treatment of aged APP23 mice. *Front. Neurosci.* **12**, 55 (2018).

61. D. G. Blackmore *et al.*, Multimodal analysis of aged wild-type mice exposed to repeated scanning ultrasound treatments demonstrates long-term safety. *Theranostics* **8**, 6233–6247 (2018).

62. M. E. Karakatsani *et al.*, Unilateral focused ultrasound-induced blood-brain barrier opening reduces phosphorylated tau from the rTg4510 mouse model. *Theranostics* **9**, 5396–5411 (2019).

63. Y. Meng *et al.*, Glymphatics visualization after focused ultrasound-induced blood-brain barrier opening in humans. *Ann. Neurol.* **86**, 975–980 (2019).

64. M. A. O'Reilly *et al.*, Investigation of the safety of focused ultrasound-induced blood-brain barrier opening in a natural canine model of aging. *Theranostics* **7**, 3573–3584 (2017).

65. A. Burgess, T. Nhan, C. Moffatt, A. L. Klibanov, K. Hynynen, Analysis of focused ultrasound-induced blood-brain barrier permeability in a mouse model of Alzheimer's disease using two-photon microscopy. *J. Control. Release* **192**, 243–248 (2014).

66. C. D. Clelland *et al.*, A functional role for adult hippocampal neurogenesis in spatial pattern separation. *Science* **325**, 210–213 (2009).

67. O. Lazarov, M. P. Mattson, D. A. Peterson, S. W. Pimplikar, H. van Praag, When neurogenesis encounters aging and disease. *Trends Neurosci.* **33**, 569–579 (2010).

68. T. Toda, F. H. Gage, Review: Adult neurogenesis contributes to hippocampal plasticity. *Cell Tissue Res.* **373**, 693–709 (2018).

69. S. J. Mooney *et al.*, Focused ultrasound-induced neurogenesis requires an increase in blood-brain barrier permeability. *PLoS One* **11**, e0159892 (2016).

70. C. Cooper, H. Y. Moon, H. van Praag, On the run for hippocampal plasticity. *Cold Spring Harb. Perspect. Med.* **8**, a029736 (2018).

71. M. K. Tobin *et al.*, Human hippocampal neurogenesis persists in aged adults and Alzheimer's disease patients. *Cell Stem Cell* **24**, 974–982.e3 (2019).

72. E. P. Moreno-Jiménez *et al.*, Adult hippocampal neurogenesis is abundant in neurologically healthy subjects and drops sharply in patients with Alzheimer's disease. *Nat. Med.* **25**, 554–560 (2019).

73. K. L. Spalding *et al.*, Dynamics of hippocampal neurogenesis in adult humans. *Cell* **153**, 1219–1227 (2013).

74. B. Gong *et al.*, IVIG immunotherapy protects against synaptic dysfunction in Alzheimer's disease through complement anaphylatoxin C5a-mediated AMPA-CREB-C/EBP signaling pathway. *Mol. Immunol.* **56**, 619–629 (2013).

75. P. He *et al.*, Deletion of tumor necrosis factor death receptor inhibits amyloid beta generation and prevents learning and memory deficits in Alzheimer's mice. *J. Cell Biol.* **178**, 829–841 (2007).

76. P. Chakrabarty, A. Herring, C. Ceballos-Diaz, P. Das, T. E. Golde, Hippocampal expression of murine TNFα results in attenuation of amyloid deposition in vivo. *Mol. Neurodegener.* **6**, 16 (2011).

77. D. E. Spaner *et al.*, Association of blood IgG with tumor necrosis factor-alpha and clinical course of chronic lymphocytic leukemia. *EBioMedicine* **35**, 222–232 (2018).

78. T. Berger *et al.*, Predicting therapeutic efficacy of intravenous immunoglobulin (IVIG) in individual patients with relapsing remitting multiple sclerosis (RRMS) by functional genomics. *J. Neuroimmunol.* **277**, 145–152 (2014).

79. G. Naert, S. Rivest, A deficiency in CCR2+ monocytes: The hidden side of Alzheimer's disease. *J. Mol. Cell Biol.* **5**, 284–293 (2013).

80. J. Quandt, K. Dorovini-Zis, The beta chemokines CCL4 and CCL5 enhance adhesion of specific CD4+ T cell subsets to human brain endothelial cells. *J. Neuropathol. Exp. Neurol.* **63**, 350–362 (2004).

81. M. Haskins, T. E. Jones, Q. Lu, S. K. Bareiss, Early alterations in blood and brain RANTES and MCP-1 expression and the effect of exercise frequency in the 3xTg-AD mouse model of Alzheimer's disease. *Neurosci. Lett.* **610**, 165–170 (2016).

82. M. I. Kester *et al.*, Decreased mRNA expression of CCL5 [RANTES] in Alzheimer's disease blood samples. *Clin. Chem. Lab. Med.* **50**, 61–65 (2011).

83. W. A. Banks, From blood-brain barrier to blood-brain interface: New opportunities for CNS drug delivery. *Nat. Rev. Drug Discov.* **15**, 275–292 (2016).

84. S. Biesmans *et al.*, Peripheral administration of tumor necrosis factor-alpha induces neuroinflammation and sickness but not depressive-like behavior in mice. *BioMed Res. Int.* **2015**, 716920 (2015).

85. D. K. Lahiri *et al.*, Role of cytokines in the gene expression of amyloid beta-protein precursor: Identification of a 5′-UTR-binding nuclear factor and its implications in Alzheimer's disease. *J. Alzheimers Dis.* **5**, 81–90 (2003).

86. M. Yamamoto *et al.*, Interferon-γ and tumor necrosis factor-α regulate amyloid-β plaque deposition and β-secretase expression in Swedish mutant APP transgenic mice. *Am. J. Pathol.* **170**, 680–692 (2007).

87. G. Liao, M. Zhang, E. W. Harhaj, S. C. Sun, Regulation of the NF-kappaB-inducing kinase by tumor necrosis factor receptor-associated factor 3-induced degradation. *J. Biol. Chem.* **279**, 26243–26250 (2004).

88. R. E. Iosif *et al.*, Tumor necrosis factor receptor 1 is a negative regulator of progenitor proliferation in adult hippocampal neurogenesis. *J. Neurosci.* **26**, 9703–9712 (2006).

89. T. L. Sudduth, A. Greenstein, D. M. Wilcock, Intracranial injection of Gammagard, a human IVIg, modulates the inflammatory response of the brain and lowers Aβ in APP/PS1 mice along a different time course than anti-Aβ antibodies. *J. Neurosci.* **33**, 9684–9692 (2013).

90. C. Cavanagh *et al.*, Inhibiting tumor necrosis factor-α before amyloidosis prevents synaptic deficits in an Alzheimer's disease model. *Neurobiol. Aging* **47**, 41–49 (2016).

91. I. Mahar *et al.*, Phenotypic alterations in hippocampal NPY- and PV-expressing interneurons in a presymptomatic transgenic mouse model of Alzheimer's disease. *Front. Aging Neurosci.* **8**, 327 (2016).

92. A. Hanna *et al.*, Age-related increase in amyloid plaque burden is associated with impairment in conditioned fear memory in CRND8 mouse model of amyloidosis. *Alzheimers Res. Ther.* **4**, 21 (2012).

93. N. P. Ellens *et al.*, The targeting accuracy of a preclinical MRI-guided focused ultrasound system. *Med. Phys.* **42**, 430–439 (2015).

94. M. A. O'Reilly, K. Hynynen, Ultrasound and microbubble-mediated blood-brain barrier disruption for targeted delivery of therapeutics to the Brain. *Methods Mol. Biol.* **1831**, 111–119 (2018).

95. M. A. O'Reilly, K. Hynynen, Blood-brain barrier: Real-time feedback-controlled focused ultrasound disruption by using an acoustic emissions-based controller. *Radiology* **263**, 96–106 (2012).

96. Y. Meng, K. Hynynen, N. Lipsman, Applications of focused ultrasound in the brain: From thermoablation to drug delivery. *Nat. Rev. Neurosci.*, 10.1038/s41582-020-00418-z (2020).